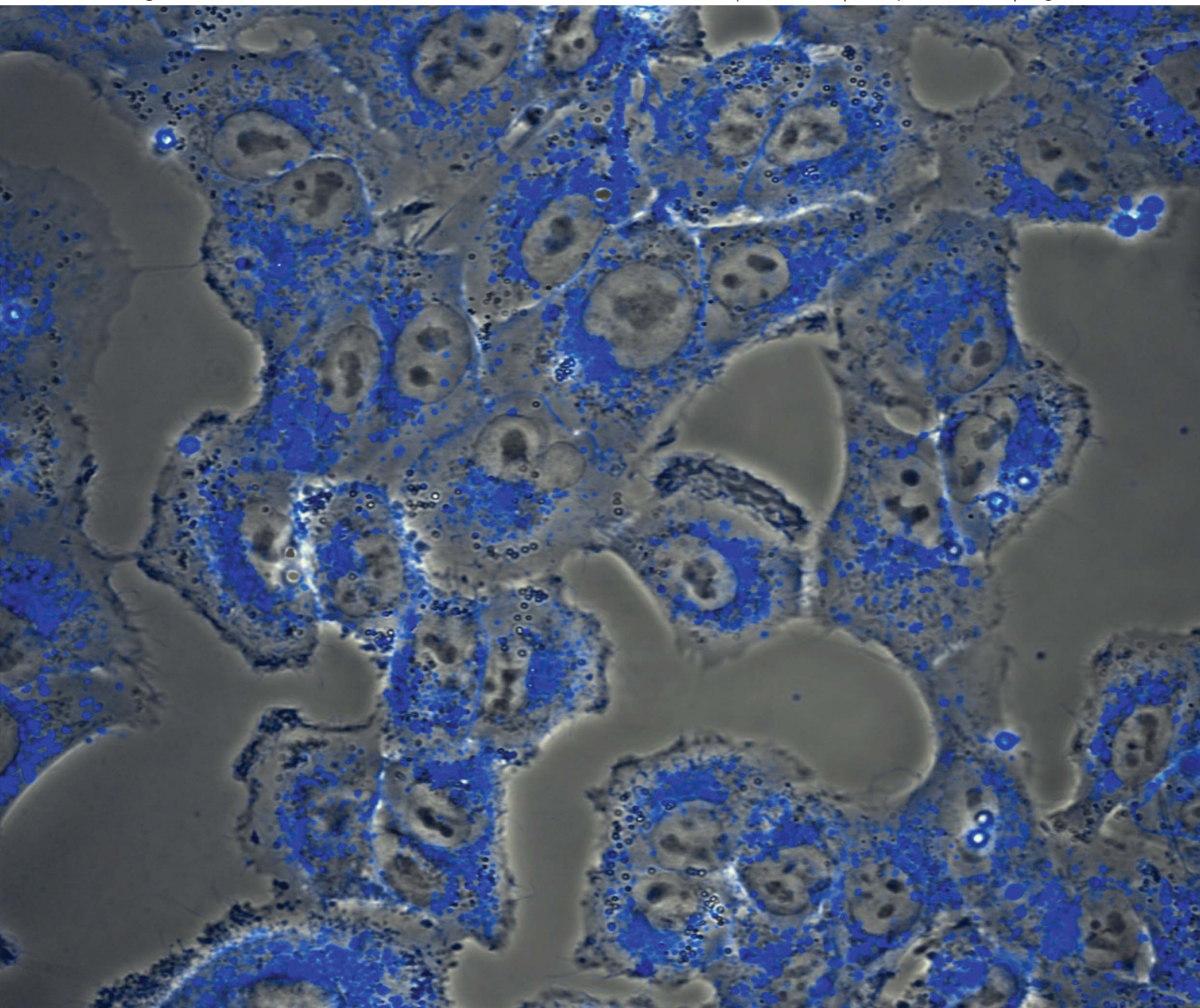


Journal of Materials Chemistry B

Materials for biology and medicine

www.rsc.org/MaterialsB

Volume 1 | Number 36 | 28 September 2013 | Pages 4523–4702



ISSN 2050-750X

RSC Publishing

PAPER

Stephen H. Foulger *et al.*
Protein triggered fluorescence switching of near-infrared emitting nanoparticles
for contrast-enhanced imaging



2050-750X(2013)1:36;1-Q

Protein triggered fluorescence switching of near-infrared emitting nanoparticles for contrast-enhanced imaging†

Cite this: *J. Mater. Chem. B*, 2013, **1**, 4542

Ragini Jetty,^a Yuriy P. Bandera,^a Michael A. Daniele,^a David Hanor,^a Hsin-I. Hung,^c Venkat Ramshesh,^c Megan F. Duperreault,^c Anna-Liisa Nieminen,^c John J. Lemasters^{cd} and Stephen H. Foulger^{*ab}

Sub-100 nm colloidal particles which are surface-functionalized with multiple environmentally-sensitive moieties have the potential to combine imaging, early detection, and the treatment of cancer with a single type of long-circulating “nanodevice”. Deep tissue imaging is achievable through the development of particles which are surface-modified with fluorophores that operate in the near-infrared (NIR) spectrum and where the fluorophore's signal can be maximized by “turning-on” the fluorescence only in the targeted tissue. We present a general approach for the synthesis of NIR emitting nanoparticles that exhibit a protein triggered activation/deactivation of the emission. Dispersing the particles into an aqueous solution, such as phosphate buffered saline (PBS), resulted in an aggregation of the hydrophobic fluorophores and a cessation of emission. The emission can be reinstated, or activated, by the conversion of the surface-attached fluorophores from an aggregate to a monomeric species with the addition of an albumin. This activated probe can be deactivated and returned to a quenched state by a simple tryptic digestion of the albumin. The methodology for emission switching offers a path to maximize the signal from the typically weak quantum yield inherent in NIR fluorophores.

Received 14th May 2013

Accepted 18th July 2013

DOI: 10.1039/c3tb20681e

www.rsc.org/MaterialsB

1 Introduction

Optical imaging in medical applications is especially attractive due to its noninvasive nature, though it can be hindered by limitations of resolution and penetration depth which are a result of the high absorption, auto fluorescence, and scattering found in biological tissues. To circumvent some of these issues, there is an interest in developing near-infrared (NIR) fluorophores since there is a region of reduced absorption for this wavelength range, providing maximum penetration of light and facilitating deep tissue imaging.¹ Unfortunately, the quantum yield of organic NIR fluorophores is typically low (<0.2) in physiological conditions^{2,3} and routes to achieve a higher tumor to background signal ratio (TBR) are desirable. Achieving a higher TBR can be accomplished by both preferentially

accumulating the probe in a targeted tissue and, once sequestered, activating the probe's fluorescence only in this region.⁴⁻⁶

A myriad of activation schemes have been proposed,^{5,7} though the approach was initially demonstrated with polymeric agents that emitted a signal after an enzymatic attack.^{6,8} The underlying mechanism for activation is a conversion of an aggregated quenched fluorophore back to its emissive monomeric state. To that end, the significant variations in the emission spectra of photoluminescent dyes which are routinely observed when they form supramolecular host/guest assemblies or complex with biomacromolecules⁹⁻¹² and have been exploited in designing activatable contrast agents by this group¹³ as well as others.¹⁴ As indicated earlier, in addition to activating the emission only in the tissue of interest, to achieve maximum TBR, the contrast agent must accumulate in the targeted tissue while clearing rapidly from non-target organs and tissues. Small molecule fluorophores are rapidly cleared because of a short *in vivo* circulation life due to non-specific binding to proteins,² thus improving the tumor to background ratio, but this also reduces the absolute amount of accumulation at the target. This weak accumulation is in addition to a limited aqueous solubility which frustrates parenteral administration.¹⁵

Compared with conventional molecular scale fluorophores, dye-doped particles have demonstrated improved *in vivo* detection and enhanced targeting efficiencies through longer

^aCenter for Optical Materials Science and Engineering Technologies, Department of Materials Science & Engineering, Clemson University, Clemson, SC 29634-0971, USA. E-mail: foulger@clemson.edu

^bDepartment of Bioengineering, Clemson University, Clemson, SC 29634-0971, USA

^cDepartment of Pharmaceutical & Biomedical Sciences, Medical University of South Carolina, Charleston, SC 29425, USA

^dDepartment of Biochemistry & Molecular Biology, Medical University of South Carolina, Charleston, SC 29425, USA

† Electronic supplementary information (ESI) available. See DOI: 10.1039/c3tb20681e

circulation times, designed clearance pathways, and multimeric binding capacities.¹⁶ Since the initial report on isolating fluorophores through their encapsulation in a particle was presented,¹⁷ a multitude of efforts have been described, using both polymeric^{18,19} and inorganic^{20–26} colloids. Sub-100 nm sized colloidal particles that are functionalized with multiple moieties have the potential to combine imaging, early detection, prevention, and the treatment of cancer with a single type of colloidal “nanodevice”.^{27–31} Within the nanodevice conceptualization, the design of a sub-100 nm particle that exhibits NIR fluorescence that can be modulated on or off by specific proteins within a cancer cell is of particular interest.^{13,14}

In the current effort, poly(propargyl acrylate) (PA) colloids were surface modified with an azide terminated squaraine-based dye, a NIR emitting fluorophore, and polyethylene glycol through a copper-catalyzed azide/alkyne cycloaddition performed in water.³² The placement of the fluorophore onto the surface of the particles allows for the dye to form a guest/host complex with available proteins and this feature was exploited in achieving a fluorescence activation of the particles when in a quenching aqueous medium. In addition, the removal of the bound proteins from the particle was achieved through their enzymatic digestion, resulting in a deactivation of the emission. Reversibility may be a crucial feature if these probes are intended for real-time monitoring of *in vivo* events. These particles described a “fluorescent switch” that can be modulated on or off through the incorporation of simple proteins and/or enzymes and are a promising platform for developing protein or multi-protein complex sensitive contrast agents for biotechnology and biomedical applications.

2 Experimental

2.1 Reagents and solvents

All the commercial reagents were purchased from TCI America and used without further purification. All the solvents were dried according to standard methods. Deionized water was obtained from a Thermo Scientific Barnstead NANOpure Water Purification System and exhibited a resistivity of *ca.* 10¹⁸ ohm⁻¹ cm⁻¹.

2.2 Chemical characterization methods

¹H and ¹³C NMR spectra were recorded on JEOL ECX-300 spectrometers (300 MHz for proton and 76 MHz for carbon). Chemical shifts for protons are reported in parts per million downfield from tetramethylsilane and are referenced to residual protium in the NMR solvent (CDCl₃: δ 7.26 ppm, DMSO-d₆: δ 2.50 ppm). Chemical shifts for carbons are reported in parts per million downfield from tetramethylsilane and are referenced to the carbon resonances of the solvent (CDCl₃: δ 77.16, DMSO-d₆: δ 39.52 ppm). Coupling constants are reported in Hertz (Hz). LC/MS mass spectra were obtained using Finnigan LCQ spectrometer and HP 1100 (HPLC). The IR spectra were recorded at room temperature in the wavenumber range of 400–4000 cm⁻¹ and referenced against air with a Nicolet 6700 FTIR instrument. A total of 32 scans were averaged for each sample at 2 cm⁻¹ resolution.

2.3 Preparation of azide-modified squaraine derivative chromophore (azSQ) (Fig. 1)

3-(3-Azidopropyl)-1,1,2-trimethyl-1H-benzo[e]indolium iodide (1). The solution containing 2,3,3-trimethyl-4,5-benzo-3H-indole (1 g, 4.78 mmol) and 1-azido-3-iodopropane (2 g, 9.56 mmol) in acetonitrile (50 mL) was refluxed for 72 hours. The solvent was evaporated under vacuum and the residue was dissolved in dichloromethane (10 mL). This solution was added drop-wise to diethyl ether solution (80 mL) to precipitate the product. This purification step with diethyl ether solution was performed 3 times and the solid obtained was filtered and dried under vacuum (hygroscopic). Compound **1** was obtained as a dark-brown solid (1.61 g, yield 80%). ¹H NMR (CDCl₃) δ 1.87 (s, 6H), 2.37 (m, 2H, *J* = 5.9 and 6.9), 3.25 (s, 3H), 3.76 (t, 2H, *J* = 5.9), 5.00 (t, 2H, *J* = 6.9), 7.70 (m, 3H, *J* = 8.6 and 1.4), 7.96 (d, 1H, *J* = 8.9), 8.10 (m, 2H, *J* = 8.6 and 8.9).

4-(1,1,2-Trimethyl-1H-benzo[e]indolium-3-yl)butane-1-sulfonate (2). The mixture containing 2,3,3-trimethyl-4,5-benzo-3H-indole (0.6 g, 2.87 mmol) and 1,4-butanediol (1.17 g, 8.59 mmol) was heated at 120 °C for 2 hours. After cooling, the crystallized product was washed with acetone, filtered and dried to give the compound (2). White solid (0.92 g, yield 93%). ¹H NMR (DMSO-d₆) δ 1.75 (s, 6H), 1.78 (m, 2H, *J* = 7.2), 2.03 (m, 2H, *J* = 7.6), 2.52 (t, 2H, *J* = 7.2), 2.95 (s, 3H), 4.61 (t, 2H, *J* = 7.6), 7.69–7.80 (m, 2H, *J* = 8.3), 8.20 (d, 2H, *J* = 8.9), 8.27 (d, 1H, *J* = 8.9), 8.36 (d, 1H, *J* = 8.3).

3,4-Diethoxy-3-cyclobutene-1,2-dione (3) was prepared according to the method published.³³

3-[(2E)-3-(3-Azidopropyl)-1,1-dimethyl-1H,2H,3H-benzo[e]indol-2-ylidene]methyl-4-hydroxycyclobut-3-ene-1,2-dione (4). Pyridine (2 mL) was added to the solution containing compound (1) (0.3 g, 0.71 mmol) and 3,4-diethoxy-cyclobut-3-ene-1,2-dione (1 g, 5.9 mmol) in ethanol (10 mL) and refluxed for 4 hours. After cooling, the green solution was evaporated and the residue was dissolved in a mixture of methanol (20 mL) and water solution of NaOH (3 mL, 0.9 mol). This mixture was refluxed for 30 min. After cooling, the mixture was filtered and evaporated. The residue was extracted with dichloromethane and washed with water 2 times. The organic layer was separated, dried with Na₂SO₄ and filtered. The filtrate was evaporated and the residue was dissolved in dichloromethane (2 mL) and added dropwise to diethyl ether solution (20 mL) to precipitate a green solid. This solid was separated by centrifugation and dried on air to give a mix of compounds (4) and (5) with molar ratio 1 : 2. This mixture (225 mg) was used in next step without further purification. ¹H NMR (CDCl₃) δ 1.93 (s, 6H), 2.14 (m, 2H), 3.40 (t, 2H, *J* = 6.0), 3.98 (t, 2H, *J* = 6.0), 5.72 (s, 1H), 7.20 (d, 1H, *J* = 8.5), 7.47 (m, 1H), 7.82 (m, 2H), 8.07 (d, 1H, *J* = 8.5).

2-[(1E)-3-[(2Z)-3-(3-Azidopropyl)-1,1-dimethyl-1H,2H,3H-benzo[e]indol-2-ylidene]methyl]-2-hydroxy-4-oxocyclobut-2-en-1-ylidene]methyl-1,1-dimethyl-3-(4-sulfonatobutyl)-1H-benzo[e]indol-3-ium (6). The mixture of compounds (4) and (5) (225 mg) (see synthesis of compound (4)) and compound (2) (140 mg, 0.4 mmol) was dissolved in butanol (15 mL) and benzene (15 mL). This solution was refluxed with Dean–Stark apparatus for 18 hours. After cooling, the solvent was evaporated under vacuum

and the residue was purified by flash column chromatography (dichloromethane : methanol 9 : 1, silica gel). 120 mg of compound (7) (a deep blue solid) was obtained. $R_f = 0.2$, yield 24% (recalculated to compound (1)). $^1\text{H NMR}$ (DMSO- d_6) δ 1.80 (m, 4H), 1.96 (s, 6H), 1.97 (s, 6H), 2.02 (m, 2H, $J = 6.6$), 2.55 (t, 2H), 3.55 (t, 2H, $J = 6.6$), 4.26 (b.t, 2H), 5.89 (s, 1H), 5.90 (s, 1H), 7.45 (m, 2H), 7.62 (m, 2H), 7.69 (d, 1H, $J = 9.0$), 7.75 (d, 1H, $J = 9.0$), 8.02 (m, 4H), 8.23 (d, 2H, $J = 8.4$). $^{13}\text{C NMR}$ (CDCl_3) δ 22.45, 26.36, 26.60, 26.80, 29.81, 40.71, 43.77, 48.63, 51.22, 51.28, 86.12, 87.10, 109.88, 110.64, 122.45, 124.20, 124.36, 127.19, 127.34, 128.33, 128.61, 129.69, 129.97, 131.17, 131.44, 133.94, 134.59, 139.17, 139.55, 170.81, 172.53. ESI-mass (LC/MS) (m/z ; rel. intensity): 715.3 (M^+ ; 100), 987.2 (8) 632.2 (8), 330.2 (17).

2.4 Preparation of azide-modified polyethylene glycol (azPEG)

The azPEG was prepared according to the method published.¹³

Mono-methoxy-PEG5000-methansulfonate. Methylsulfonyl chloride (0.92 g, 8 mmol) in dichloromethane (5 mL) was added dropwise at room temperature to the stirring solution of triethylamine (0.89 g, 8.8 mmol) and mono-methoxy-PEG5000 (20 g, 4 mmol) in dichloromethane (70 mL). The solution was

stirred at 20 °C for 4 hours, then washed with water and the organic layer was dried with Na_2SO_4 with further filtration. The solvent was evaporated under vacuum to give the product as a white solid. Yield: 20.3 g (97%). $^1\text{H NMR}$ (CDCl_3) 3.07 (s, 3H), 3.36 (s, 3H), 3.48 (t, 2H), 3.53 (m, 2H), 3.62 (m, *ca.* 400H), 3.75 (m, 4H), 4.36 (m, 2H).

Mono-methoxy-PEG5000-azide. The mixture of mono-methoxy-PEG5000-methansulfonate (20.3 g, 4 mmol) and sodium azide (1.1 g, 17 mmol) in acetonitrile (80 mL) was refluxed and stirred for 15 hours. After cooling, the mixture was filtered and the solvent was evaporated. The residue was dissolved in dichloromethane and washed with water, organic layer was separated, dried with Na_2SO_4 and filtered. The solvent was evaporated, the crystalline residue was washed with hexane, filtered and dried in air to give the product as a white solid. Yield: 19 g (94%). $^1\text{H NMR}$ (CDCl_3) 3.35 (s, 3H), 3.38 (t, 2H), 3.62 (m, *ca.* 400H), 3.85 (m, 2H). FTIR (cm^{-1}): 1095 (s, C–O–C); 1340, 1465 (CH_2); 2100 (N_3); 2880 (s, CH_2).

2.5 Preparation of the particles

Propargyl acrylate (PA) particles were prepared according to a standard emulsion polymerization method published.¹³

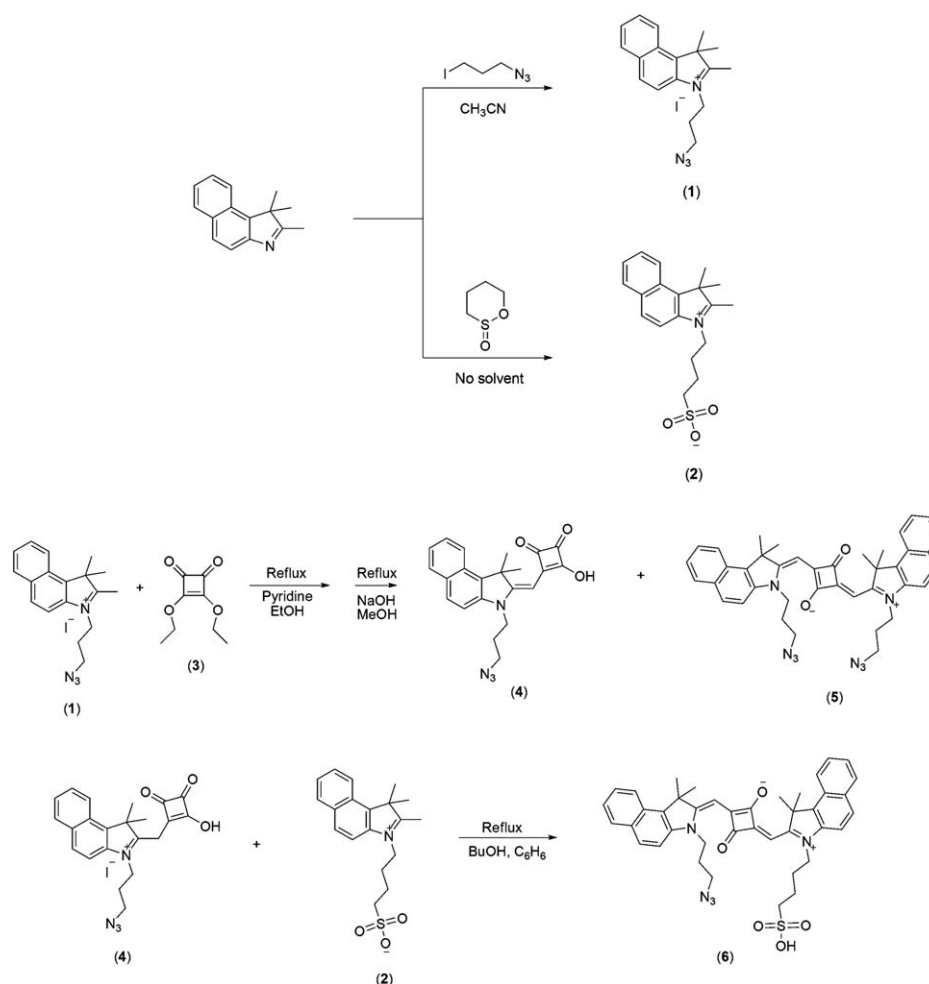


Fig. 1 Reaction scheme for synthesis of azSQ.

For a typical surface modification of the particles, for example, the grafting of azSQ and azide-modified PEG chains with molecular weight of 5000 (azPEG) onto the particles, 1 mL PA particles and 3.94 mg azSQ were added to 2 mL of deionized water. Solutions of 0.07624 g copper(II) sulfate (99.999% Aldrich) in 10 mL deionized water and 0.3024 g sodium ascorbate (99% Aldrich) in 10 mL deionized water were made. Initially, 0.5 mL of the CuSO₄ solution was added to the PA/azSQ solution, followed by 0.5 mL of the sodium ascorbate solution. The resulting mixture was maintained at a temperature of *ca.* 28 °C for 15 minutes and then the reaction was stopped by the removal of unreacted azSQ, sodium ascorbate, and Cu(II)SO₄ through a repeated particle washing procedure consisting of centrifugation and redispersion in methanol. The cleaned PA/azSQ (FP₅) particles in water were subsequently utilized in a secondary click transformation with 54.99 mg azPEG, and previously presented CuSO₄ and sodium ascorbate solutions. The reaction was allowed to run for 48 hours and then washed to remove unreacted species as determined by photoluminescence measurements; these particles are referred to as PA/azSQ/azPEG (FP₇) particles.

2.6 Cell analysis

Human HepG2 and A549 cell lines were obtained from ATCC (Rockville, MD). Human UMSCC22A head and neck squamous carcinoma cell line was a gift from Dr Besim Ogretmen (Medical University of South Carolina). HepG2 cells were cultured in phenol red-free Dulbeccos modified Eagles media (DMEM) containing 5% fetal bovine serum (FBS), 1% penicillin–streptomycin, and supplemented with glutamine (Invitrogen, Carlsbad, CA). A549 cells were cultured in F-12K media (Kaighn's Modification of Ham's F-12 medium) containing 10% fetal bovine serum (FBS) and 1% penicillin–streptomycin. UMSCC22A cells were cultured in Dulbeccos modified Eagles media (DMEM) supplemented with L-glutamine containing 10% FBS and 1% penicillin–streptomycin. Cells were cultured at 37 °C in a humidified atmosphere of 95% air 5% CO₂.

2.7 Cytotoxicity assay

HepG2 cells & A549 (20 000 cells per well) were cultured on 96 well plates for 24 hours. Subsequently, cells were, exposed to 2×10^9 , 2×10^{11} , and 2×10^{13} particles per mL. After 96 hours, cell death was assessed with a MTS assay according to the manufacturer's instructions (Promega, Madison, WI). Briefly, medium was aspirated and a solution of 100 μL of DMEM containing 10% FBS and 20 μL 3-(4,5-dimethylthiazol-2-yl)-5-(3-carboxymethoxyphenyl)-2-(4-sulfophenyl)-2H-tetrazolium, salt (MTS) and phenazine methosulfate (PMS) was added onto each well. After 60 minutes, wells were scanned colorimetrically at 490 nm on a VersaMax spectrophotometer (Molecular Devices, Sunnyvale, CA). The conversion of MTS into an aqueous soluble formazan product is achieved only by dehydrogenase enzymes which are present in metabolically active cells; the absorbance at 490 nm from the formazan product is directly proportional to the number of living cells in culture.

2.8 Confocal microscopy

UMSCC22A cells were cultured onto 35 mm glass-bottomed Petri dishes (MatTek Corporation, Ashland, MA) at 150 000 cells per dish and incubated for 24 hours. Subsequently, cells were incubated with 1 μM PA/azSQ/azPEG (FP₇) particles for different time periods of 1, 2, 4, 8, 17, and 24 hours. At the end of the incubation, the medium was aspirated and the cells were incubated with 500 nM LysoTracker Green (LTG) for 1 hour. Before imaging the concentration of the LTG dye was lowered to 100 nM. Dishes were placed in an environmental chamber at 37 °C on the stage of Olympus FV10i LIV laser scanning confocal microscope. The images of LTG (473 nm excitation and 490–540 nm emission) and FP₇ particles (635 nm excitation and 660–760 nm emission) were collected using a 63 × N.A. 1.4 oil immersion planapochromat objective. ImageJ software was used to post-process the images and calculate the co-localization coefficients.

2.9 Optical characterization methods

Absorption spectra were taken using a Perkin-Elmer Lambda 900 UV/VIS/NIR spectrophotometer. Photoluminescence (PL) spectra were collected using a Photon Technology International QuantaMaster 60 NIR with PMT spectrofluorometer and a Thermo Oriel xenon arc lamp (Thermo Oriel 66902) mated with a Thermo Oriel Cornerstone 7400 1/8 m monochromator (Thermo Oriel 7400) and a Horiba Jobin-Yvon MicroHR spectrometer coupled to a Synapse CCD detector. Quantum yields (ϕ) of the dyes and modified particles were determined relative to the reference dye 1,1',3,3',3',3'-hexamethylindotricarbocyanine iodide (HITCI) in methanol, which has a fluorescence quantum yield of $\phi_{\text{ref}} = 0.12$,^{34,35} employing established procedures.³⁶ It is to be noted that the diameter of the particles used through out the paper was 49.9 nm except for quantum yield measurement where a couple of particles of diameter 88.5 nm were used.

3 Results & discussion

A schematic of the particles studied in this effort is presented in Fig. 2. The poly(propargyl acrylate) (PA) colloids were prepared using a standard aqueous emulsion polymerization technique resulting in spheres with a diameter of 49.9 ± 0.58 nm (mean and standard deviation). To functionalize the surface of the particles, a multiple step copper-catalyzed azide/alkyne cycloaddition ("click" transformation) was performed in water³² to produce PA particles that had both squaraine and polyethylene glycol (PEG) attached to their surface. Initially, an azide-modified squaraine derivative (azSQ) was attached to the PA particles through a "click" transformation. Squaraine dyes are typically classified as a NIR dye though technically their emission is in the far-red regime.^{37–40} Due to their high fluorescent quantum yields compared to other NIR organic fluorophores like indocyanine green,^{13,41} squaraine dyes have found a broad range of applications,^{33,37,42} with the biomedical community expressing an especially strong interest in this class of dyes.^{38–40,43,44}

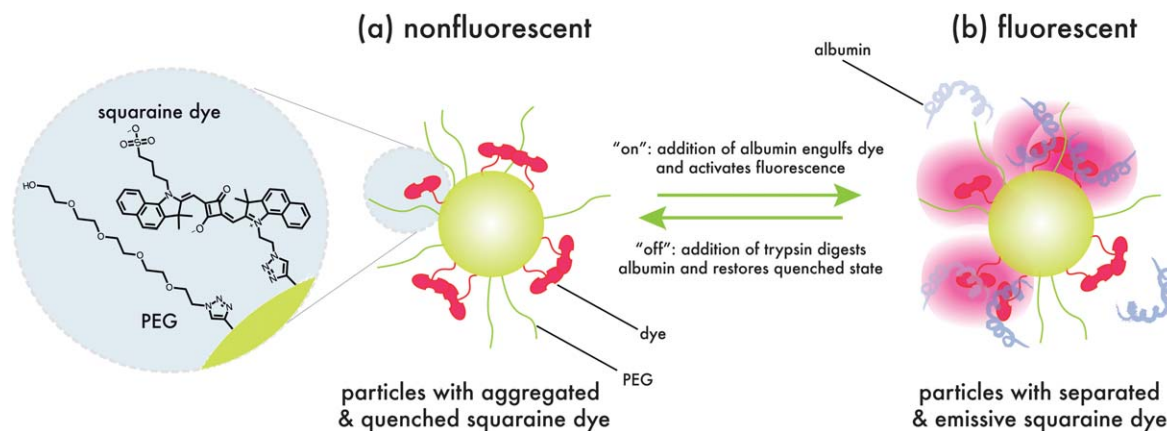


Fig. 2 Schematic of 50 nm poly(propargyl acrylate) (PA) particles surface modified with an azide-terminated squaraine (azSQ) and polyethylene glycol (azPEG) through an aqueous-phase “click” transformation in the (a) aggregated & nonfluorescent state and in the (b) albumin activated fluorescent state. Particles could be deactivated and returned to the quenched state through a trypsin digestion of the albumin.

To attach the fluorophores to the particles, the azSQ was initially clicked onto the particles for 15 min and then the reaction was stopped by the removal of unreacted azSQ, sodium ascorbate, and Cu(II)SO_4 through a repeated particle washing procedure consisting of centrifugation and redispersion in methanol. To reduce the grafting density of dye, the initial amount of azide-modified dye used in the reaction was decreased. The cleaned PA/azSQ (FP₅) particles were subsequently utilized in a secondary click transformation with azide-modified polyethylene glycol chains with molecular weight of 5k (azPEG) that was allowed to run for 48 hours and then washed to remove unreacted species; these particles are referred to as PA/azSQ/azPEG (FP₇) particles. The use of PEG to infer a hydrophilicity to the particles has been found to be important for directing protein absorption on the particles and achieving long circulation times.¹⁶ The characteristics of the particles synthesized for this study are presented in Table 1.

3.1 Emission spectrum

Fig. 3a presents the molar extinction coefficient and photoluminescence of the free azide-functionalized squaraine (azSQ) dispersed in methanol. In this solvent, azSQ has a peak absorption maximum at 663 nm, while the corresponding emission peak is at 672 nm, for a relatively small Stokes shift of 9 nm. The symmetry for the absorption and emission spectra is evident, though the absorption exhibits a small peak at 626 nm. This lower energy absorption is often seen in concentrated aqueous solutions of squaraine due to the formation of H-aggregates;^{44,45} the appearance of this peak in the freshly prepared dilute methanol solution of azSQ is due to the sulfonate group which causes higher self-affinity.⁴⁶

A structurally similar squaraine dye has been recently presented⁴⁷ that was characterized by an absorption and emission peak maximum of 672 nm and 678 nm, respectively, when dispersed in toluene. In this solvent, this dye gave a fluorescence quantum yield of 0.51. In comparison, the relative fluorescence quantum yield for azSQ in toluene differed by 0.1%

when measured in methanol ($\phi = 0.101$; *cf.* Table 1). Despite the minor solvent-dependent changes in the spectra between this latter squaraine dye and azSQ, the fluorescence quantum yield of the azSQ is significantly lower at 0.101. The reduction in quantum yield was speculated to be due to the substitution of an azide to the chromophore and its ability to better facilitate non-radiative deactivation to the ground state.⁴⁶

In comparison, Fig. 3b presents the absorption and photoluminescence spectra of PA particles after they have been surface modified with the attachment of azSQ chromophores and azPEG chains (FP₇) and dispersed in methanol. The absorption spectra of the FP₇ particles indicate an absorption peak maximum that is at a wavelength of *ca.* 672 nm, a 9 nm bathochromic shift from the free dye. Utilizing the molar extinction coefficient in the dilute regime for the free azSQ particles in methanol (*cf.* Fig. 3a) allows for the estimation of the number of chromophores attached to the particles. Following this approach, the FP₇ particles had a grafting density of 0.49 azSQ per nm² when analyzed over the wavelength range of 615 nm to 685 nm. The grafting density of the azPEG to the particles was not assessed but the contact angle of the PA particles to water changed from $\theta > 70^\circ$ to $\theta < 10^\circ$ after the

Table 1 Fluorophore grafting density and fluorescence quantum yield (ϕ) of surface functionalized PA particles; fluorophore and particles dispersed in methanol

Compound	Fluorophore grafting density (azSQ per nm ²)	Quantum yield (ϕ)
azSQ	—	0.101
FP ₀	PA/azSQ	0.05
FP ₁	PA/azSQ	0.09
FP ₂	PA/azSQ	0.12
FP ₃	PA/azSQ	0.17
FP ₄	PA/azSQ	0.28
FP ₅	PA/azSQ	0.49
FP ₆	PA/azSQ/azPEG	0.09
FP ₇	PA/azSQ/azPEG	0.49

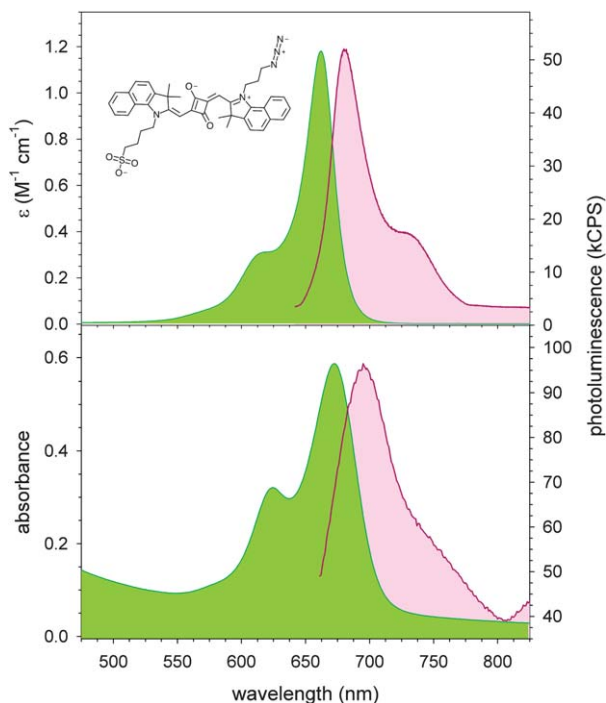


Fig. 3 (a) Molar extinction coefficient (green) and photoluminescence (red) of azide functionalized squaraine derivative chromophore (azSQ; 6.98 μM in methanol); (b) absorbance (green) and photoluminescence (red) of PA/azSQ/azPEG (FP₇) particles in methanol. Excitation energy at a wavelength of 630 nm.

attachment of the azPEG indicating that their surface was hydrophilic.

3.2 Quantum yield

It is well known that when fluorophores are dispersed in a solvent that a limiting concentration can be found where the dye–dye separation becomes small and statistical closely spaced pairs and larger aggregates are formed.³⁵ Once excited, these aggregates can find non-radiative routes to lower their energy, thereby reducing the observed luminescence quantum yield. Once the chromophores are attached to the surface of particles, the “local” concentration of the emitters is elevated due to the two-dimensional nature of the attachment. This elevated concentration of emitters results in an enhanced propensity for aggregate formation and non-radiative routes for the excited emitters to return to their ground state. Therefore, the counter intuitive speculation is that a *reduced* number of chromophores grafted to a particle’s surface will result in a higher quantum yield. Table 1 and Fig. 4 presents the quantum yield for the “free” azide-functionalized squaraine derivative dye and the modified particles with varying fluorophore grafting densities. In addition, Table 1 presents a subset of the PA/azSQ particles clicked with an azide-modified PEG.

As indicated earlier, the free azSQ dye exhibited a quantum yield of $\phi = 0.101$. Once the chromophores are attached to a particle, the observed quantum yield was significantly diminished relative to the free dye’s value (*cf.* Fig. 4). The PA/azSQ particles (FP₅; *cf.* Table 1) with a dye grafting density of 0.49

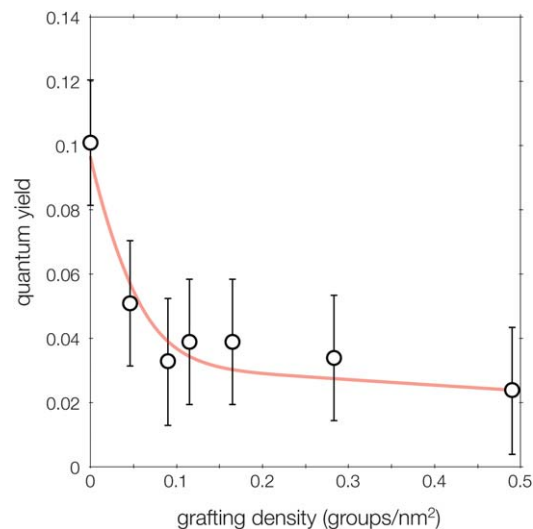


Fig. 4 Quantum yield of azide functionalized squaraine derivative chromophore (azSQ) with variation in grafting density to PA particles (methanol). Excitation energy at a wavelength of 650 nm.

groups per nm² exhibits a 76% drop in quantum yield relative to the free dye, while the PA/azSQ particles (FP₁; *cf.* Table 1) with a grafting density of 0.09 groups per nm² exhibits a 67% drop in quantum yield. The particles may act as quenching centers of fluorescence for chromophores that are adsorbed onto their surface since (1) the planar surface offers a constrained 2-dimensional region on which the chromophores can dimerize⁴⁸ and (2) a non-radiative energy transfer can occur from the excited molecules to the particle.³⁵ As speculated earlier, the reduction of the number of fluorophores grafted onto the particle’s surface results in an increase in quantum yield (*cf.* Table 1). For the PA/azSQ particles, a 37% reduction in grafting density, from 0.49 to 0.09 groups per nm², results in a 38% increase in quantum yield. The azSQ dye can be roughly approximated as an ellipsoid with a long axis of 21 Å and a cross section of 10 Å × 5 Å. At a grafting density of 0.49 groups per nm², the inter-dye separation distance on the surface of the particle would be statistically 16 Å. This distance is sufficiently close that two dyes could approach one another to partially dimerize and reduce the quantum yield of emission. In contrast, a grafting density of 0.09 groups per nm² gives a separation distance of *ca.* 38 Å, a distance sufficiently large enough to frustrate dye–dye aggregation.

It is well established that PEG polymers, when attached to the surface of particles, provide steric stabilization and reduces protein absorption in biomedical applications.⁴⁹ Protein absorption promotes opsonization, which can lead to aggregation and clearance from the bloodstream. The resultant rapid removal is due to phagocytosis by the mononuclear phagocyte system (MPS) in the liver and splenic filtration.⁵⁰ Nonetheless, the addition of PEG chains to the surface of the particles reduces the quantum yield of the particles. Table 1 presents the fluorescence quantum yield of the particle with varying grafting densities and PEGylation. At higher grafting densities, the quantum yield of the FP₇ particles was half of the PEG-free FP₅

particles, while at the lower grafting densities (FP₁ & FP₆), the PEGylation did not effect the yield significantly. This suggests that the attachment of the PEG chains increases the non-radiative transfer of energy when excited, and hence influences the emission characteristics of the attached squaraine.

3.3 Squaraine/protein complexation

The utilization of an azSQ-modified particle for any *in vivo* or *in vitro* imaging application will require the particles to be dispersed in an aqueous environment. The replacement of methanol for a PBS solution in the FP₇ particles resulted in a total quenching of fluorescence (*cf.* Fig. 5a). Due to the hydrophobic nature of the dye, the employment of PBS is speculated to force the bound azSQ to sequester to the particle surface and dimerize.^{35,51}

It has been established that the fluorescence quantum yield of squaraine dyes can change when the dye is adsorbed onto macromolecules such as proteins and enzymes,^{44,52} and this response can be employed as a fluorescent diagnostic probe in medical and biological applications. Previous studies have established that squaraine adsorption occurs on the *ca.* 10 nm sized human albumin protein and that dye adsorption will dominate over dye dimerization when the dye number density is less than a few times the protein number density.⁵² In the current system, the FP₇ particles in water were mixed with bovine serum albumin (BSA) at concentration of 0.05 mM. The emission intensity in Fig. 5a exhibited an immediate increase within the first 30 minutes that accounted for *ca.* 25% of the total increase in intensity followed by a long-term gradual increase. Even though the emission turn-on occurred in just a few minutes, the change in intensity was monitored over a 4 day incubation period to insure it had plateaued. At BSA

concentration of *ca.* 0.05 mM, the number of BSA molecules is approximately equal to 15.4 times the total number of azSQ in the system. There was a 1991% increase in output intensity at the peak wavelength of 687 nm, while the total integrated intensity was *ca.* 10 times greater. As indicated in Fig. 5a, the study was also performed with human serum albumin (HSA) instead of BSA and the fluorescence enhancement with the human variant was identical to the bovine version. A similar study was performed with the enzymes, lysozyme and trypsin, and with the surfactant, sodium dodecyl sulfate (SDS). The surfactant was successful in breaking up the aggregation of the fluorophores and activating the fluorescence of the particles,¹⁴ while the lysozyme and trypsin were not (*cf.* ESI†). Serum albumin is a major protein constituent of blood plasma and this protein facilitates the disposition and transport of a variety of exogenous and endogenous ligands to specific regions. The delivery of ligands originates from two (BSA) and one (HSA) structurally selective binding site(s) where the binding affinity originates from a combination of hydrophobic, hydrogen bonding, and electrostatic interactions. The observed increase in fluorescence intensity with BSA and HSA binding likely results from the ability of the protein to “dissolve” hydrophobically aggregated azSQ on the surface of the particles.^{39,52} In addition, tight binding to the protein environment, possibly at the hydrophobic pockets, may increase the molecular rigidity of the dye, which reduces the vibrational modes and further raises the fluorescence signal.²

The most commonly used NIR probes, organic fluorescent dyes, are often chemically unstable and susceptible to bleaching by the attack of nucleophiles that are abundant in biological environments.⁵³ An approach to overcome this deficiency is through steric protection of the fluorophore by forming a rotaxane with the dye^{37,43,54} or encapsulation inside a

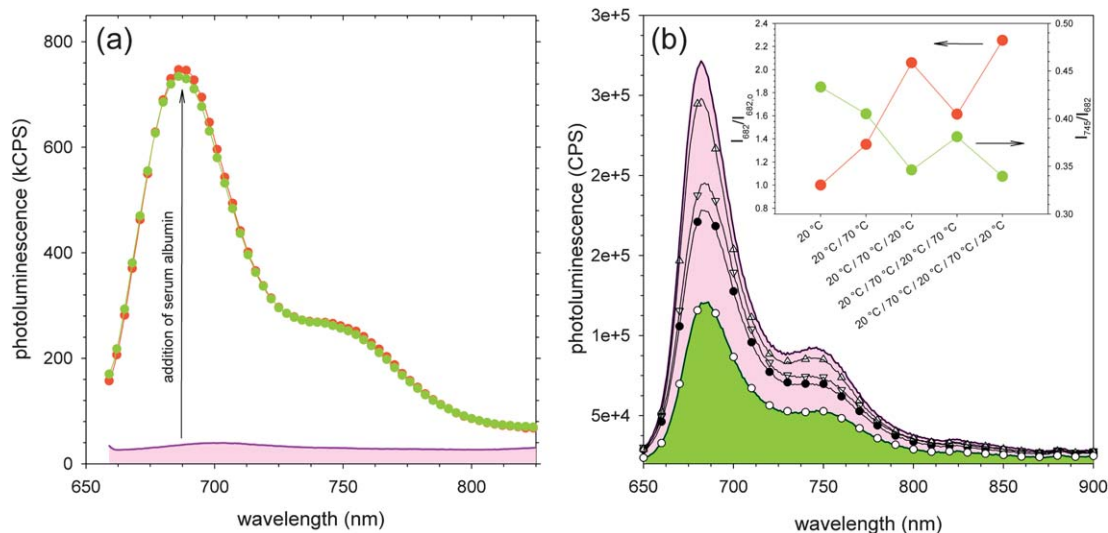


Fig. 5 (a) Photoluminescence of FP₇ particles dispersed in: PBS (—), PBS and 0.05 mM BSA (green), PBS and 0.05 mM HSA (red). Particles were incubated with serum albumin for *ca.* 4 days to insure increase was invariant with time, though 25% of the increase occurred within the first 30 minutes. (b) Photoluminescence spectra of FP₅ particles in PBS with 15 mg BSA initially at 20 °C (O), at 70 °C (●), after 70 °C anneal then cooled to 20 °C (Δ), after 70 °C, cool to 20 °C, heated to 70 °C (▽), and after 70 °C, cool to 20 °C, heated to 70 °C, then cooled to 20 °C (—). Inset presents the intensity ratio at 682 nm (red) for the thermal cycles relative to the initial emission and the intensity ratio (green) of the J-aggregates (745 nm) to the monomeric emission (682 nm). Excitation energy at a wavelength of 630 nm.

particle.^{17–21} The former approach requires sophisticated chemistry to thread the dye through the macrocyclic cavity, usually resulting in a low yield, while the latter approach negates the prospect of forming beneficial guest/host assemblies with the fluorophore. The simpler and more versatile approach is the physical entrapment of the hydrophobic fluorophore inside the hydrophobic pockets of an aqueous dispersible protein or vesicle.⁴⁰ Fig. 6 presents the normalized change in fluorescence intensity of the free azSQ dye and FP₇ particles incubated with BSA, all dispersed in water, with exposure to hydrogen peroxide, an effective nucleophile. The drop in observed fluorescence intensity of the free dye is due to the degradation of the fluorophore by the hydrogen peroxide, while the fluorophores that are within the hydrophobic pocket of the BSA (or merely engulfed) continue to fluoresce even at much higher concentrations of hydrogen peroxide. It appears that the fluorophore/protein complex that activates the fluorophore's emission is possibly preventing the ingress of the hydrogen peroxide to the dye or acting as a scavenger for the peroxide.^{55,56}

BSA has been indicated to initiate irreversible unfolding at temperatures greater than 60–70 °C.⁵⁷ Below this temperature, in the folded state, the protein exhibits global translational and rotational diffusion, but when above this temperature, the protein undergoes structural changes which are accompanied by changes in the protein dynamics.^{58,59} Fig. 5b presents the increase in fluorescence when the FP₅ particles that are dispersed in PBS, have been incubated with BSA and undergo thermal cycling at temperatures above the irreversible unfolding temperature of BSA. At temperatures in the denaturation regime, the proteins initially unfold and extend, and if the proximity to one another is sufficiently high, the unfolded protein chains can entangle and potentially partially cross-link.⁵⁸ As indicated earlier, the incubation of the aqueous-phase particles with BSA results in a dramatic turn-on in emission intensity of 1.2×10^5 counts per second at 682 nm (*cf.* Fig. 5a).

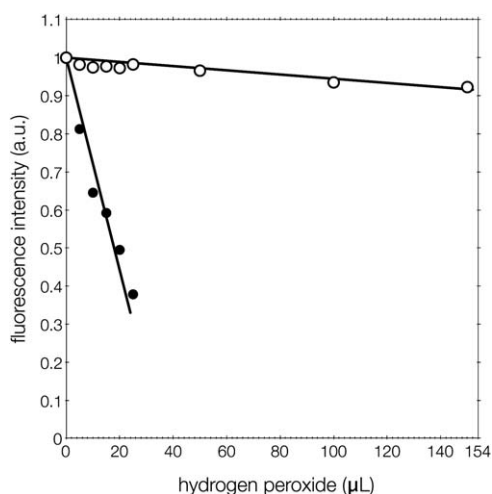


Fig. 6 Change in fluorescence intensity at wavelength of 671 nm with exposure to hydrogen peroxide of free azSQ dye (●) and FP₇ particles incubated with BSA (○). Aqueous solution with excitation energy at a wavelength of 630 nm.

Raising the temperature to 70 °C results in a 35% enhancement of the emission, though once the particles are cooled to 20 °C, the emission increases by 105% (at 682 nm). An additional annealing cycle results in a total increase in emission intensity of 125% (*cf.* Fig. 5b inset). The absolute increase in emission with annealing is dependent on both the ratio of azSQ to BSA as well as their thermal history. Nonetheless, there is a significant change in the emission characteristics with annealing.

In comparison to the “monomeric” absorbance, squaraine dyes that are dispersed in aqueous solutions tend to form aggregates that exhibit an absorbance that has a bathochromic (J-aggregates) or hypsochromic (H-aggregates) shift. These aggregates also affect the emission properties, with H-aggregates usually being poor emitters and J-aggregates often giving efficient fluorescence.⁴⁴ The inset in Fig. 5b presents the intensity ratio of the J-aggregates (745 nm) to the monomeric emission (682 nm) and suggests a conversion of the aggregates to the monomeric form with thermal cycling; a conclusion that is corroborated with the absorption characteristics (*cf.* ESI†). Due to the steric limitations of the azSQ being tethered to the surface of the particle, J-aggregates are characterized structurally as having only one end of the azSQ aligned with the end ring of the other azSQ. The large fluorescence turn-on associated with the conversion of the surface-attached azSQ fluorophores from “aggregate to monomeric species” may be attributed to the inclusion of the dye into the hydrophobic pocket of BSA when in its native folded form. The fluorescent enhancement of the particles when they are thermally cycled above the denaturing temperature of BSA suggests that other factors than just a pocket-based complexation is operative in converting the dye molecules from their non-emissive aggregate states to the fluorescent monomeric form. The unfolded state may offer opportunities of the protein to bind to additional fluorophores on the surface of the particle, reducing the non-radiative decay rate of the fluorescent molecules and raising the fluorescence signal.^{60,61} The PEGylated particles, FP₆ & FP₇, did not exhibit such a dramatic increase in photoluminescence with annealing. The FP₇ particles exhibited a modest 13% increase in integrated intensity with annealing and it is speculated that the PEG chains are effective in preventing the unfolded BSA from finding, adhering to, and destroying fluorophore aggregates.

A number of reports have demonstrated the “activation” of NIR particles through the embodiment of a guest/host complexation on the surface of the particles.^{13,14} Recently, particles surface functionalized with azadipyrromethenes had their emission turned-on when mixed with either an anionic or nonionic surfactant, as well as a phospholipid.¹⁴ Our laboratory has recently demonstrated the BSA activation of indocyanine green (ICG) functionalized particles.¹³ These studies both accomplished the activation of emission through the formation of a guest/host complex, yet there has been no methodology to deactivate the emission. To this end, the use of a protein in our studies allows for its digestion once on the particle and a route to deactivate the fluorescence. Fig. 7 presents the fluorescence activation/deactivation of FP₅. These particles were equilibrated with 0.025 mM BSA in a Tris–HCl buffer of pH 8, then annealed at 65 °C and cooled to 20 °C. The annealing step was repeated

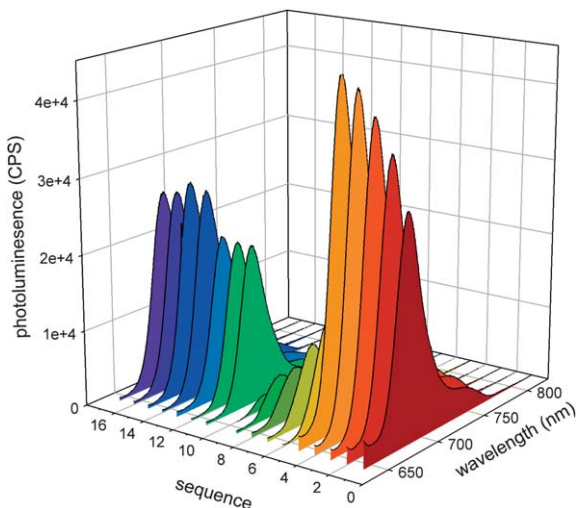


Fig. 7 Variation of photoluminescence spectrum of FP_5 particles in PBS incubated with BSA (sequence 0), with four annealing cycles (sequence 1–5), with introduction & incubation of trypsin (sequence 6–10), reintroduction & incubation of BSA (sequence 11–13) and with four annealing cycles (sequence 14–17). Excitation energy at a wavelength of 630 nm. An annealing cycle consists of raising the sample temperature to 65 °C for 20 min and then returning the temperature to 20 °C.

four times. As demonstrated previously (*cf.* Fig. 5b), the annealing resulted in a significant enhancement in the emission intensity. Mixing the particles with trypsin (0.143 mM), a standard enzyme used for the digestion of albumin, and incubating the mixture at 37 °C for 15 hours resulted in a 71% drop in emission, while after 64 hours the decrease was 85% complete. With 184 hours of incubation there was an almost complete cessation of emission. The majority of the emission turn-off was complete in a few minutes, the reaction was monitored over a substantial incubation period (*ca.* 7.6 days) to insure a plateau was reached. Trypsin catalyses the hydrolysis of peptide bonds so that albumin is broken into smaller peptides and it is speculated that the fragments from BSA are unable to effectively “coat” the azSQ and these chromophores again coalesce and quench on the surface of the particles. Performing the same digestion study with particles that had not been annealed resulted in a similar response, though the fluorescence deactivation was not as complete. It is speculated that the BSA is more structurally open after annealing and trypsin is more effective in digesting the denatured protein.^{62,63} Once again adding an excess of BSA to the FP_5 particles after the trypsin digestion results in a return to the approximate initial emission intensity after 48 hours of incubation, though the trypsin was not removed from the system and would continue to digest the BSA, preventing a full return to the initial emission characteristics. In addition, an UV/Vis absorption study confirmed that the particles could not recover all of their initial emission intensity after an annealing & digestion study due to a slight degradation of the fluorophores (*cf.* ESI†).³⁷ The repeated turn-on and turn-off of the fluorescence is demonstrated in Fig. 7, which presents the change in the photoluminescence spectrum with annealing of the FP_5 particles with BSA to activate and enhance the

emission, exposure to trypsin to deactivate the emission, and a subsequent introduction of BSA again to reactivate the emission. The annealing resulted in a 48% increase in the number of active emitters and an increase in the relative quantum yield to 0.036 from 0.024, while the trypsin digestion turned-off 97% of the emitters and dropped the relative quantum yield to 7.2×10^{-4} . Similarly, the PEGylated particles, FP_5 & FP_7 , exhibited an almost complete cessation of emission with tryptic digestion of the BSA. The FP_7 particles exhibited an eleven-fold increase integrated intensity with BSA activation, that was improved 13% with annealing. The introduction of trypsin returned the particles to a quenched state within just a few hours of the enzyme addition.

3.4 *In vitro* co-localization

In medical diagnostics, one of the problems limiting the use of many small molecule fluorophores is the difficulty in preparing pharmaceutical formulations that are amenable to parenteral administration.¹⁵

The majority of organic chromophores that are of interest are not soluble in water and cannot be simply injected. To remedy this, a number of different approaches, including encapsulation of the fluorophore in colloidal carriers such as oil-dispersions, liposomes, and polymeric particles, have been investigated.^{43,54,64,65} The encapsulation in an aqueous dispersible particle allows for the straightforward insertion of the fluorophore into the patient but prevents the formation of any advantageous guest/host complexes with the chromophore and a target protein.

The surface-attachment of the fluorophore onto the particle insures its accessibility to proteins but may alter the ability of the particles to penetrate cells of interest. To that end, the cellular uptake and intracellular trafficking of the FP_7 particles (*cf.* Table 1) were studied by live cell confocal laser scanning microscopy. In addition, cell viability studies were carried out with the A549 and HepG2 cell lines and the FP_7 particles were deemed not cytotoxic at the concentrations used in this study (*cf.* ESI†).

The particles were incubated with UMSCC22A head and neck cancer cells and confocal images of the cells were collected after 1, 8, and 17 h of incubation with particles (*cf.* Fig. 8); the particles' fluorescence was activated by fetal bovine serum (FBS) in the culture medium. We labeled the lysosomes with LysoTracker Green (LTG), which stains acidic compartments such as late endosomes and lysosomes, to study the co-localization between the lysosomes and particles. The fluorescence of the particles co-localized with the LTG (Fig. 8), indicating that the particles were taken up by the cells through endocytosis and accumulated into the lysosomes. The FP_7 particles were also incubated with A549 cells which are a human alveolar adenocarcinoma cell line. These cells synthesize lecithin with a high percentage of disaturated fatty acids and are believed to be responsible for pulmonary surfactant synthesis.⁶⁶ Fig. 9 presents a confocal image of the FP_7 emission channel overlaid on the transmitted image of the A549 cancer cells. The particles were incubated with the cells without FBS and were initially

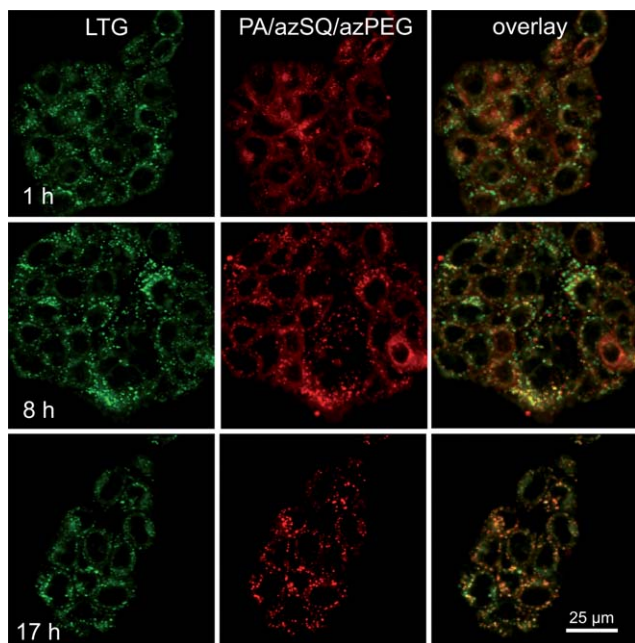


Fig. 8 Confocal images of FP_7 particles ($1 \mu M$) incubated with UMSCC22A cells for 1, 8, and 17 hours. One hour before imaging, cells were loaded with Lyso-Tracker Green (LTG) to image lysosomes. LTG (green, 473 nm) is left image, PA/azSQ/azPEG particles (red, FP_7) is the center image, and the right image is their overlay.

nonfluorescent, but after 30 minutes of incubation the particles were fluorescent as they collected onto the cell membranes (*cf.* Fig. 9); the fluorescence is clearly evident by 1 hour of incubation as the particles begin to be engulfed by the cells. In this study, no FBS was utilized in the medium and the fluorescence was activated by constituents of the cells. This fluorescence turn-on is speculated to be due to the phospholipids in the cell membrane, specifically lecithin, and is mechanistically similar to the use of the surfactant SDS to activate the fluorophores.¹⁴

For the co-localization study with the UMSCC22A cancer cells, the Manders' co-localization coefficient M_1 and M_2 (ref. 67) for the FP_7 particles and LTG increased in a time-dependent manner and after 17 hours, the co-localization coefficient has risen to *ca.* 0.75 (*cf.* Fig. 10). The relative equivalence of the coefficients (M_1 or M_2) at any sampled time suggests that the particle/LTG emitter ratio is not changing significantly, though

the slight increase (0.07) in M_2 (red channel) relative to M_1 (green channel) at longer times could indicate a reduction in the number of emitting FP_7 particles. Since the lysosomes constitute the intracellular digestion compartment, the observed co-localization between the lysosomes and the FP_7 particles should result in the degradation of the fluorescence activating FBS that is absorbed on the particles and result in a return of the particles to a quenched state. Fig. 9 presents confocal images of the FP_7 emission channel overlaid on the transmitted image of the A549 cells. As discussed earlier, since no FBS was added to the cell's media, the fluorescence activation of the particles was accomplished by the phospholipids in the cell membrane, specifically lecithin production of the cells binding to the fluorophores and reducing their aggregate-based quenching. At 2 hours of incubation (*cf.* Fig. 9), the FP_7 particles have migrated into the lysosomes and there is a high density of FP_7 emitters in the cells. Over the course of an additional 22 hours of incubation (*cf.* Fig. 9), the number of FP_7 emitters appears to be diminishing, consistent with the trypsin digestion study of Fig. 7. In order to estimate the number of emitters per cancer cell, images of the cells at 17 and 24 hours had a common threshold applied to the red channel and the number of pixels above the threshold were counted. Following this

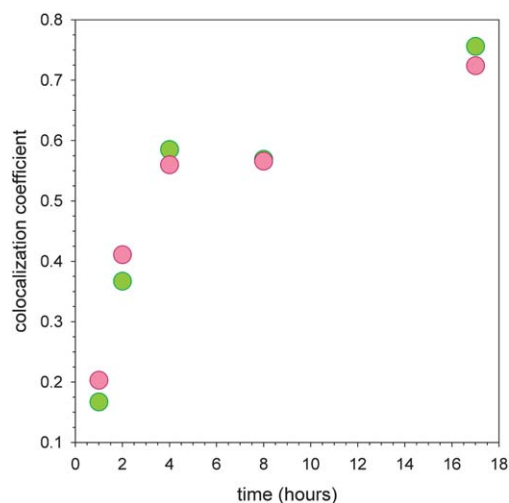


Fig. 10 Manders' co-localization coefficient M_1 (green channel) and M_2 (red channel) from Fig. 8 of FP_7 particles incubated with UMSCC22A cells.

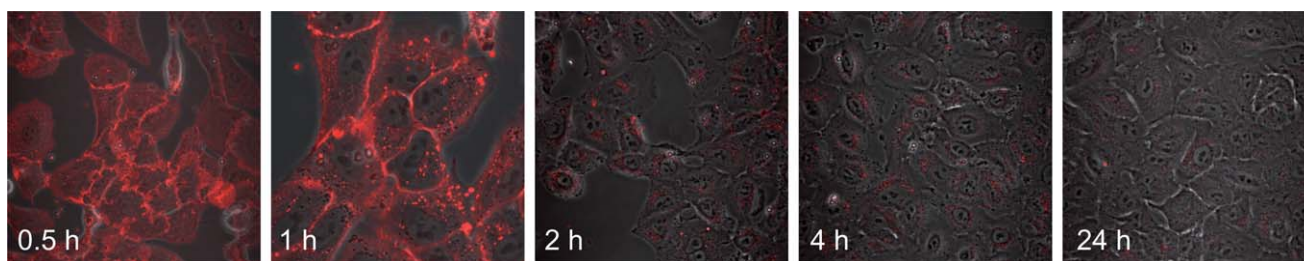


Fig. 9 Confocal images of FP_7 particles ($1 \mu M$) incubated with A549 cancer cells depicting the activation of fluorescence with incubation time (0.5–1 h) and subsequent reduction in fluorescence with incubation time (2–24 h) as particles enter lysosomes. Media did not contain FBS and excitation laser power was constant between images.

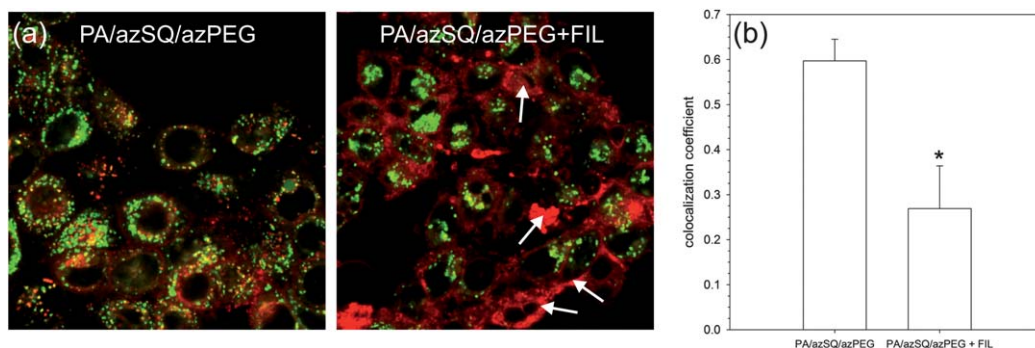


Fig. 11 (a) Confocal images of FP₇ particles (1 μM) incubated with UMSCC22A cells for 2 hours (left image) and with the addition of the raft/caveolae endocytosis pathway inhibitor filipin (FIL) (right image) and corresponding (b) Pearson's co-localization coefficient between LTG and FP₇ particles. An asterisk indicates statistical significance from the control by ANOVA followed by Tukeys multiple comparisons test ($p < 0.01$).

procedure, the cells incubated for 17 hours had 691 pixels per cell above the threshold, while the cells incubated for 24 hours had only 167 pixels per cell, a 75% reduction. All *in vitro* studies with the particles indicate that the rapid emission turn-off is not due to merely dye degradation. Similarly to the previously described tryptic digestion study, we speculate that the phospholipids which are sequestered on the particles are being removed once the particles localize in the lysosomes and the adherent can no longer prevent the chromophores from aggregating and quenching their emission.

There are multiple mechanisms of endocytosis that can be utilized for penetration of nanoparticles into cells. A pharmacologic approach was used to determine which mechanism of endocytosis was involved in cellular uptake of the FP₇ particles in UMSCC22A cells. A number of compounds, when incubated with mammalian cells, disrupt specific routes of endocytosis. For example, cytochalasin D inhibits macropinocytosis, chlorpromazine inhibits clathrin-mediated endocytosis by inhibiting disassembly of clathrin-coated pits and inhibiting receptor recycling to the plasma membrane, nocodazole inhibits clathrin- and caveolae-independent endocytosis by disrupting microtubules, and filipin III inhibits caveolae-mediated endocytosis by sequestering cholesterol available for lipid rafts. When cytochalasin D, chlorpromazine, and nocodazole were initially added to the UMSCC22A cells 30 min before the addition of the FP₇ particles, no change in the final Pearson's co-localization coefficient between LTG and the FP₇ particles were seen. In contrast, filipin (FIL) had a significant influence on the coefficient. Fig. 11a presents confocal images of the cells incubated with the FP₇ particles without the inhibitor of the raft/caveolae endocytosis pathway and with the compound (FIL). Confocal images revealed patches of nanoparticles bound to the plasma membrane in filipin-treated cells (arrows), indicating that filipin prevented FP₇ particles from entering cells. The inclusion of the filipin decreased the Pearson's co-localization coefficient by *ca.* 50% (*cf.* Fig. 11b). The results indicate that the nanoparticles are taken up by the cells through caveolae-mediated endocytosis for a final intracellular destination at the lysosomes. A number of studies have found that nontargeted particles follow a caveolae-mediated endocytosis route from early endosomes to late endosomes and lysosomes.^{68–70}

4 Conclusions

The 50 nm poly(propargyl acrylate) particles which were surface modified through the copper-catalyzed azide/alkyne cycloaddition of an azide-terminated squaraine derivative, a near-infrared emitter, and polyethylene glycol exhibited a protein triggered activation/deactivation of the emission. When dispersed in PBS, the initially nonfluorescent particles exhibited an albumin-based activation which resulted in an eleven-fold enhancement in integrated intensity. Deactivation with the addition of trypsin to cleave the albumin resulted in a complete return to the initial quenched state. Quenched NIR emitting particles which can have their emission activated by their exposure to a specific protein, then deactivated by exposure to another protein, are a potentially valuable nanodevice for the fight against cancer. A new generation of photonic imaging systems will be created from adaptive & responsive contrast mechanisms using highly specific fluorescent agents, such as activated fluorescent probes described in this effort, when these probes are leveraged with the recent advances in illumination & detection schemes, tomographic principles, and mathematical models that describe photon propagation in tissues.⁷¹

Acknowledgements

The authors thank the Gregg-Graniteville Foundation for financial support. The research was supported by grants from the US National Cancer Institute, R01 CA119079 (ALN), P30 CA138313 (Hollings Cancer Center Cell and Molecular Imaging Shared Resource) and Abney Cancer Foundation (H-I H).

References

- 1 S. A. Hilderbrand and R. Weissleder, *Curr. Opin. Chem. Biol.*, 2010, **14**, 71–79.
- 2 S. A. Soper and Q. L. Mattingly, *J. Am. Chem. Soc.*, 1994, **116**, 3744–3752.
- 3 A. K. Chibisov, G. V. Zakharova, H. Gorner, Y. A. Sogulyaev, I. L. Mushkalo and A. I. Tolmachev, *J. Phys. Chem.*, 1995, **99**, 886–893.

- 4 Y. Hama, Y. Urano, Y. Koyama, P. L. Choyke and H. Kobayashi, *Cancer Res.*, 2007, **67**, 3809–3817.
- 5 H. Kobayashi, M. R. Longmire, M. Ogawa and P. L. Choyke, *Chem. Soc. Rev.*, 2011, **40**, 4626–4648.
- 6 C. H. Tung, S. Bredow, U. Mahmood and R. Weissleder, *Bioconjugate Chem.*, 1999, **10**, 892–896.
- 7 H. Kobayashi and P. L. Choyke, *Acc. Chem. Res.*, 2011, **44**, 83–90.
- 8 R. Weissleder, C. H. Tung, U. Mahmood and A. Bogdanov, *Nat. Biotechnol.*, 1999, **17**, 375–378.
- 9 A. C. Bhasikuttan, J. Mohanty, W. M. Nau and H. Pal, *Angew. Chem., Int. Ed.*, 2007, **46**, 4120–4122.
- 10 R. Zadnani and T. Schrader, *J. Am. Chem. Soc.*, 2005, **127**, 904–915.
- 11 S. Gadde, E. K. Batchelor, J. P. Weiss, Y. H. Ling and A. E. Kaifer, *J. Am. Chem. Soc.*, 2008, **130**, 17114–17119.
- 12 A. Toutchkine, V. Kraynov and K. Hahn, *J. Am. Chem. Soc.*, 2003, **125**, 4132–4145.
- 13 P. Rungta, Y. P. Bandera, R. D. Roeder, Y. C. Li, W. S. Baldwin, D. Sharma, M. G. Sehorn, I. Luginov and S. H. Foulger, *Macromol. Biosci.*, 2011, **11**, 927–937.
- 14 A. Palma, L. A. Alvarez, D. Scholz, D. O. Frimannsson, M. Grossi, S. J. Quinn and D. F. O'Shea, *J. Am. Chem. Soc.*, 2011, **133**, 19618–19621.
- 15 R. G. Strickley, *Pharm. Res.*, 2004, **21**, 201–230.
- 16 S. M. Moghimi, A. C. Hunter and J. C. Murray, *Pharmacol. Rev.*, 2001, **53**, 283–318.
- 17 D. Avnir, D. Levy and R. Reisfeld, *J. Phys. Chem.*, 1984, **88**, 5956–5959.
- 18 J. M. Devoisselle, S. Soulie-Begu, S. Mordon, T. Desmettre and H. Maillols, *Laser Med. Sci.*, 1998, **13**, 279–282.
- 19 J. Yu, M. A. Yaseen, B. Anvari and M. S. Wong, *Chem. Mater.*, 2007, **19**, 1277–1284.
- 20 E. I. Altinoglu, T. J. Russin, J. M. Kaiser, B. M. Barth, P. C. Eklund, M. Kester and J. H. Adair, *ACS Nano*, 2008, **2**, 2075–2084.
- 21 H. S. Muddana, T. T. Morgan, J. H. Adair and P. J. Butler, *Nano Lett.*, 2009, **9**, 1559–1566.
- 22 A. Burns, H. Ow and U. Wiesner, *Chem. Soc. Rev.*, 2006, **35**, 1028–1042.
- 23 S. Kim, T. Y. Ohulchanskyy, H. E. Pudavar, R. K. Pandey and P. N. Prasad, *J. Am. Chem. Soc.*, 2007, **129**, 2669–2675.
- 24 Y. Piao, A. Burns, J. Kim, U. Wiesner and T. Hyeon, *Adv. Funct. Mater.*, 2008, **18**, 3745–3758.
- 25 Y. Ueno, J. Jose, A. Loudet, C. Perez-Bolivar, P. Anzenbacher and K. Burgess, *J. Am. Chem. Soc.*, 2011, **133**, 51–55.
- 26 J. Yu, D. Javier, M. A. Yaseen, N. Nitin, R. Richards-Kortum, B. Anvari and M. S. Wong, *J. Am. Chem. Soc.*, 2010, **132**, 1929–1938.
- 27 A. K. Gupta and M. Gupta, *Biomaterials*, 2005, **26**, 3995–4021.
- 28 A. H. Lu, E. L. Salabas and F. Schuth, *Angew. Chem., Int. Ed.*, 2007, **46**, 1222–1244.
- 29 C. Medina, M. J. Santos-Martinez, A. Radomski, O. I. Corrigan and M. W. Radomski, *Br. J. Pharmacol.*, 2007, **150**, 552–558.
- 30 W. H. De Jong and P. J. A. Borm, *Int. J. Nanomed.*, 2008, **3**, 133–149.
- 31 V. P. Torchilin, *Adv. Drug Delivery Rev.*, 2006, **58**, 1532–1555.
- 32 H. C. Kolb, M. G. Finn and K. B. Sharpless, *Angew. Chem., Int. Ed.*, 2001, **40**, 2004–2021.
- 33 J. H. Yum, P. Walter, S. Huber, D. Rentsch, T. Geiger, F. Nuesch, F. De Angelis, M. Gratzel and M. K. Nazeeruddin, *J. Am. Chem. Soc.*, 2007, **129**, 10320–10321.
- 34 P. Sperber, W. Spangler, B. Meier and A. Penzkofer, *Opt. Quantum Electron.*, 1988, **20**, 395–431.
- 35 R. Philip, A. Penzkofer, W. Baumler, R. M. Szeimies and C. Abels, *J. Photochem. Photobiol., A*, 1996, **96**, 137–148.
- 36 A. T. R. Williams, S. A. Winfield and J. N. Miller, *Analyst*, 1983, **108**, 1067–1071.
- 37 E. Arunkumar, C. C. Forbes, B. C. Noll and B. D. Smith, *J. Am. Chem. Soc.*, 2005, **127**, 3288–3289.
- 38 L. Beverina, M. Crippa, M. Landenna, R. Ruffo, P. Salice, F. Silvestri, S. Versari, A. Villa, L. Ciaffoni, E. Collini, C. Ferrante, S. Bradamante, C. M. Mari, R. Bozio and G. A. Pagani, *J. Am. Chem. Soc.*, 2008, **130**, 1894–1902.
- 39 V. S. Jisha, K. T. Arun, M. Hariharan and D. Ramaiah, *J. Am. Chem. Soc.*, 2006, **128**, 6024–6025.
- 40 D. Lee, Y. K. Lim, C. S. Kim, I. C. Kwon and J. Kim, *Adv. Funct. Mater.*, 2010, **20**, 2786–2793.
- 41 T. Desmettre, J. M. Devoisselle and S. Mordon, *Surv. Ophthalmol.*, 2000, **45**, 15–27.
- 42 S. Sreejith, P. Carol, P. Chithra and A. Ajayaghosh, *J. Mater. Chem.*, 2008, **18**, 264–274.
- 43 J. Johnson, N. Fu, E. Arunkumar, W. Leevy, S. Gammon, D. Piwnica-Worms and B. Smith, *Angew. Chem., Int. Ed.*, 2007, **46**, 5528–5531.
- 44 Y. Xu, Z. Li, A. Malkovskiy, S. Sun and Y. Pang, *J. Phys. Chem. B*, 2010, **114**, 8574–8580.
- 45 K. Y. Law, *J. Phys. Chem.*, 1987, **91**, 5184–5193.
- 46 C. L. Amiot, S. P. Xu, S. Liang, L. Y. Pan and J. X. J. Zhao, *Sensors*, 2008, **8**, 3082–3105.
- 47 P. Salice, J. Arnbjerg, B. W. Pedersen, R. Toftgaard, L. Beverina, G. A. Pagani and P. R. Ogilby, *J. Phys. Chem. A*, 2010, **114**, 2518–2525.
- 48 E. Mubarekyan and M. Santore, *Langmuir*, 1998, **14**, 1597–1603.
- 49 K. Avgoustakis, *Curr. Drug Delivery*, 2004, **1**, 321–333.
- 50 F. Alexis, E. Pridgen, L. K. Molnar and O. C. Farokhzad, *Mol. Pharmaceutics*, 2008, **5**, 505–515.
- 51 J. J. Gassensmith, J. M. Baumes and B. D. Smith, *Chem. Commun.*, 2009, 6329–6338.
- 52 V. S. Jisha, K. T. Arun, M. Hariharan and D. Ramaiah, *J. Phys. Chem. B*, 2010, **114**, 5912–5919.
- 53 A. Mishra, R. K. Behera, P. K. Behera, B. K. Mishra and G. B. Behera, *Chem. Rev.*, 2000, **100**, 1973–2011.
- 54 E. Arunkumar, C. C. Forbes and B. D. Smith, *Eur. J. Org. Chem.*, 2005, 4051–4059.
- 55 R. Pirisino, P. Disimplicio, G. Ignesti, G. Bianchi and P. Barbera, *Pharmacol. Res. Commun.*, 1988, **20**, 545–552.

- 56 C. P. Baron, H. H. F. Refsgaard, L. H. Skibsted and M. L. Andersen, *Free Radical Res.*, 2006, **40**, 409–417.
- 57 P. L. SanBiagio, D. Bulone, A. Emanuele and M. U. Palma, *Biophys. J.*, 1996, **70**, 494–499.
- 58 I. H. M. Vanstokkum, H. Linsdell, J. M. Hadden, P. I. Haris, D. Chapman and M. Bloemendal, *Biochemistry*, 1995, **34**, 10508–10518.
- 59 M. Hennig, F. Roosen-Runge, F. J. Zhang, S. Zorn, M. W. A. Skoda, R. M. J. Jacobs, T. Seydel and F. Schreiber, *Soft Matter*, 2012, **8**, 1628–1633.
- 60 R. P. Cory, R. R. Becker, R. Rosenblu and I. Isenberg, *J. Am. Chem. Soc.*, 1968, **90**, 1643.
- 61 V. H. Rees, J. E. Fildes and D. J. Laurence, *J. Clin. Pathol.*, 1954, **7**, 336–340.
- 62 D. Lopez-Ferrer, K. Petritis, K. K. Hixson, T. H. Heibeck, R. J. Moore, M. E. Belov, D. G. Camp and R. D. Smith, *J. Proteome Res.*, 2008, **7**, 3276–3281.
- 63 J. L. Capelo, R. Carreira, M. Diniz, L. Fernandes, M. Galesio, C. Lodeiro, H. M. Santos and G. Vale, *Anal. Chim. Acta*, 2009, **650**, 151–159.
- 64 J. J. Gassensmith, E. Arunkumar, L. Barr, J. M. Baumes, K. M. DiVittorio, J. R. Johnson, B. C. Noll and B. D. Smith, *J. Am. Chem. Soc.*, 2007, **129**, 15054–15059.
- 65 Y. N. Konan, R. Gurny and E. Allemann, *J. Photochem. Photobiol., B*, 2002, **66**, 89–106.
- 66 M. Lieber, B. Smith, A. Szakal, W. Nelsonrees and G. Todaro, *Int. J. Cancer*, 1976, **17**, 62–70.
- 67 V. Zinchuk and O. Zinchuk, *Curr. Protoc. Cell Biol.*, 2008, **39**, 4.19.1–4.19.16.
- 68 M. Oba, S. Fukushima, N. Kanayama, K. Aoyagi, N. Nishiyama, H. Koyama and K. Kataoka, *Bioconjugate Chem.*, 2007, **18**, 1415–1423.
- 69 M. Oba, K. Aoyagi, K. Miyata, Y. Matsumoto, K. Itaka, N. Nishiyama, Y. Yarnasaki, H. Koyama and K. Kataoka, *Mol. Pharmaceutics*, 2008, **5**, 1080–1092.
- 70 S. Hak, E. Helgesen, H. H. Hektoen, E. M. Huuse, P. A. Jarzyna, W. J. M. Mulder, O. Haraldseth and C. D. Davies, *ACS Nano*, 2012, **6**, 5648–5658.
- 71 V. Ntziachristos, J. Ripoll, L. H. V. Wang and R. Weissleder, *Nat. Biotechnol.*, 2005, **23**, 313–320.